

Combination of D0 measurements of the top quark mass

V.M. Abazov,³¹ B. Abbott,⁶⁷ B.S. Acharya,²⁵ M. Adams,⁴⁶ T. Adams,⁴⁴ J.P. Agnew,⁴¹ G.D. Alexeev,³¹ G. Alkhazov,³⁵ A. Alton^a,⁵⁶ A. Askew,⁴⁴ S. Atkins,⁵⁴ K. Augsten,⁷ V. Aushev,³⁸ Y. Aushev,³⁸ C. Avila,⁵ F. Badaud,¹⁰ L. Bagby,⁴⁵ B. Baldin,⁴⁵ D.V. Bandurin,⁷⁴ S. Banerjee,²⁵ E. Barberis,⁵⁵ P. Baringer,⁵³ J.F. Bartlett,⁴⁵ U. Bassler,¹⁵ V. Bazterra,⁴⁶ A. Bean,⁵³ M. Begalli,² L. Bellantoni,⁴⁵ S.B. Beri,²³ G. Bernardi,¹⁴ R. Bernhard,¹⁹ I. Bertram,³⁹ M. Besançon,¹⁵ R. Beuselinck,⁴⁰ P.C. Bhat,⁴⁵ S. Bhatia,⁵⁸ V. Bhatnagar,²³ G. Blazey,⁴⁷ S. Blessing,⁴⁴ K. Bloom,⁵⁹ A. Boehnlein,⁴⁵ D. Boline,⁶⁴ E.E. Boos,³³ G. Borissov,³⁹ M. Borysova^l,³⁸ A. Brandt,⁷¹ O. Brandt,²⁰ M. Brochmann,⁷⁵ R. Brock,⁵⁷ A. Bross,⁴⁵ D. Brown,¹⁴ X.B. Bu,⁴⁵ M. Buehler,⁴⁵ V. Buescher,²¹ V. Bunichev,³³ S. Burdin^b,³⁹ C.P. Buszello,³⁷ E. Camacho-Pérez,²⁸ B.C.K. Casey,⁴⁵ H. Castilla-Valdez,²⁸ S. Caughron,⁵⁷ S. Chakrabarti,⁶⁴ K.M. Chan,⁵¹ A. Chandra,⁷³ E. Chapon,¹⁵ G. Chen,⁵³ S.W. Cho,²⁷ S. Choi,²⁷ B. Choudhary,²⁴ S. Cihangir[‡],⁴⁵ D. Claes,⁵⁹ J. Clutter,⁵³ M. Cooke^k,⁴⁵ W.E. Cooper,⁴⁵ M. Corcoran[‡],⁷³ F. Couderc,¹⁵ M.-C. Cousinou,¹² J. Cuth,²¹ D. Cutts,⁷⁰ A. Das,⁷² G. Davies,⁴⁰ S.J. de Jong,^{29,30} E. De La Cruz-Burelo,²⁸ F. Déliot,¹⁵ R. Demina,⁶³ D. Denisov,⁴⁵ S.P. Denisov,³⁴ S. Desai,⁴⁵ C. Deterre^c,⁴¹ K. DeVaughan,⁵⁹ H.T. Diehl,⁴⁵ M. Diesburg,⁴⁵ P.F. Ding,⁴¹ A. Dominguez,⁵⁹ A. Drutskoy,³² A. Dubey,²⁴ L.V. Dudko,³³ A. Duperrin,¹² S. Dutt,²³ M. Eads,⁴⁷ D. Edmunds,⁵⁷ J. Ellison,⁴³ V.D. Elvira,⁴⁵ Y. Enari,¹⁴ H. Evans,⁴⁹ A. Evdokimov,⁴⁶ V.N. Evdokimov,³⁴ A. Fauré,¹⁵ L. Feng,⁴⁷ T. Ferbel,⁶³ F. Fiedler,²¹ F. Filthaut,^{29,30} W. Fisher,⁵⁷ H.E. Fisk,⁴⁵ M. Fortner,⁴⁷ H. Fox,³⁹ J. Franc,⁷ S. Fuess,⁴⁵ P.H. Garbincius,⁴⁵ A. Garcia-Bellido,⁶³ J.A. García-González,²⁸ V. Gavrilov,³² W. Geng,^{12,57} C.E. Gerber,⁴⁶ Y. Gershtein,⁶⁰ G. Ginther,⁴⁵ O. Gogota,³⁸ G. Golovanov,³¹ P.D. Grannis,⁶⁴ S. Greder,¹⁶ H. Greenlee,⁴⁵ G. Grenier,¹⁷ Ph. Gris,¹⁰ J.-F. Grivaz,¹³ A. Grohsjean^c,¹⁵ S. Grünendahl,⁴⁵ M.W. Grünewald,²⁶ T. Guillemin,¹³ G. Gutierrez,⁴⁵ P. Gutierrez,⁶⁷ J. Haley,⁶⁸ L. Han,⁴ K. Harder,⁴¹ A. Harel,⁶³ J.M. Hauptman,⁵² J. Hays,⁴⁰ T. Head,⁴¹ T. Hebbeker,¹⁸ D. Hedin,⁴⁷ H. Hegab,⁶⁸ A.P. Heinson,⁴³ U. Heintz,⁷⁰ C. Hensel,¹ I. Heredia-De La Cruz^d,²⁸ K. Herner,⁴⁵ G. Hesketh^f,⁴¹ M.D. Hildreth,⁵¹ R. Hirosky,⁷⁴ T. Hoang,⁴⁴ J.D. Hobbs,⁶⁴ B. Hoeneisen,⁹ J. Hogan,⁷³ M. Hohlfield,²¹ J.L. Holzbauer,⁵⁸ I. Howley,⁷¹ Z. Hubacek,^{7,15} V. Hynek,⁷ I. Iashvili,⁶² Y. Ilchenko,⁷² R. Illingworth,⁴⁵ A.S. Ito,⁴⁵ S. Jabeen^m,⁴⁵ M. Jaffré,¹³ A. Jayasinghe,⁶⁷ M.S. Jeong,²⁷ R. Jesik,⁴⁰ P. Jiang[‡],⁴ K. Johns,⁴² E. Johnson,⁵⁷ M. Johnson,⁴⁵ A. Jonckheere,⁴⁵ P. Jonsson,⁴⁰ J. Joshi,⁴³ A.W. Jung^o,⁴⁵ A. Juste,³⁶ E. Kajfasz,¹² D. Karmanov,³³ I. Katsanos,⁵⁹ M. Kaur,²³ R. Kehoe,⁷² S. Kermiche,¹² N. Khalatyan,⁴⁵ A. Khanov,⁶⁸ A. Kharchilava,⁶² Y.N. Kharzheev,³¹ I. Kiselevich,³² J.M. Kohli,²³ A.V. Kozelov,³⁴ J. Kraus,⁵⁸ A. Kumar,⁶² A. Kupco,⁸ T. Kurča,¹⁷ V.A. Kuzmin,³³ S. Lammers,⁴⁹ P. Lebrun,¹⁷ H.S. Lee,²⁷ S.W. Lee,⁵² W.M. Lee,⁴⁵ X. Lei,⁴² J. Lellouch,¹⁴ D. Li,¹⁴ H. Li,⁷⁴ L. Li,⁴³ Q.Z. Li,⁴⁵ J.K. Lim,²⁷ D. Lincoln,⁴⁵ J. Linnemann,⁵⁷ V.V. Lipaev[‡],³⁴ R. Lipton,⁴⁵ H. Liu,⁷² Y. Liu,⁴ A. Lobodenko,³⁵ M. Lokajicek,⁸ R. Lopes de Sa,⁴⁵ R. Luna-Garcia^g,²⁸ A.L. Lyon,⁴⁵ A.K.A. Maciel,¹ R. Madar,¹⁹ R. Magaña-Villalba,²⁸ S. Malik,⁵⁹ V.L. Malyshev,³¹ J. Mansour,²⁰ J. Martínez-Ortega,²⁸ R. McCarthy,⁶⁴ C.L. McGivern,⁴¹ M.M. Meijer,^{29,30} A. Melnitchouk,⁴⁵ D. Menezes,⁴⁷ P.G. Mercadante,³ M. Merkin,³³ A. Meyer,¹⁸ J. Meyerⁱ,²⁰ F. Miconi,¹⁶ N.K. Mondal,²⁵ M. Mulhearn,⁷⁴ E. Nagy,¹² M. Narain,⁷⁰ R. Nayyar,⁴² H.A. Neal,⁵⁶ J.P. Negret,⁵ P. Neustroev,³⁵ H.T. Nguyen,⁷⁴ T. Nunnemann,²² J. Orduna,⁷⁰ N. Osman,¹² A. Pal,⁷¹ N. Parashar,⁵⁰ V. Parihar,⁷⁰ S.K. Park,²⁷ R. Partridge^e,⁷⁰ N. Parua,⁴⁹ A. Patwa^j,⁶⁵ B. Penning,⁴⁰ M. Perfilov,³³ Y. Peters,⁴¹ K. Petridis,⁴¹ G. Petrillo,⁶³ P. Pétroff,¹³ M.-A. Pleier,⁶⁵ V.M. Podstavkov,⁴⁵ A.V. Popov,³⁴ M. Prewitt,⁷³ D. Price,⁴¹ N. Prokopenko,³⁴ J. Qian,⁵⁶ A. Quadt,²⁰ B. Quinn,⁵⁸ P.N. Ratoff,³⁹ I. Razumov,³⁴ I. Ripp-Baudot,¹⁶ F. Rizatdinova,⁶⁸ M. Rominsky,⁴⁵ A. Ross,³⁹ C. Royon,⁸ P. Rubinov,⁴⁵ R. Ruchti,⁵¹ G. Sajot,¹¹ A. Sánchez-Hernández,²⁸ M.P. Sanders,²² A.S. Santos^h,¹ G. Savage,⁴⁵ M. Savitskyi,³⁸ L. Sawyer,⁵⁴ T. Scanlon,⁴⁰ R.D. Schamberger,⁶⁴ Y. Scheglov,³⁵ H. Schellman,^{69,48} M. Schott,²¹ C. Schwanenberger,⁴¹ R. Schwienhorst,⁵⁷ J. Sekaric,⁵³ H. Severini,⁶⁷ E. Shabalina,²⁰ V. Shary,¹⁵ S. Shaw,⁴¹ A.A. Shchukin,³⁴ O. Shkola,³⁸ V. Simak,⁷ P. Skubic,⁶⁷ P. Slattery,⁶³ G.R. Snow,⁵⁹ J. Snow,⁶⁶ S. Snyder,⁶⁵ S. Söldner-Rembold,⁴¹ L. Sonnenschein,¹⁸ K. Soustruznik,⁶ J. Stark,¹¹ N. Stefaniuk,³⁸ D.A. Stoyanova,³⁴ M. Strauss,⁶⁷ L. Suter,⁴¹ P. Svoisky,⁷⁴ M. Titov,¹⁵ V.V. Tokmenin,³¹ Y.-T. Tsai,⁶³ D. Tsybychev,⁶⁴ B. Tuchming,¹⁵ C. Tully,⁶¹ L. Uvarov,³⁵ S. Uvarov,³⁵ S. Uzunyan,⁴⁷ R. Van Kooten,⁴⁹ W.M. van Leeuwen,²⁹ N. Varelas,⁴⁶ E.W. Varnes,⁴² I.A. Vasilyev,³⁴ A.Y. Verkhnev,³¹ L.S. Vertogradov,³¹ M. Verzocchi,⁴⁵ M. Vesterinen,⁴¹ D. Vilanova,¹⁵ P. Vokac,⁷ H.D. Wahl,⁴⁴ M.H.L.S. Wang,⁴⁵ J. Warchol,⁵¹ G. Watts,⁷⁵ M. Wayne,⁵¹ J. Weichert,²¹ L. Welty-Rieger,⁴⁸ M.R.J. Williamsⁿ,⁴⁹ G.W. Wilson,⁵³ M. Wobisch,⁵⁴ D.R. Wood,⁵⁵ T.R. Wyatt,⁴¹ Y. Xie,⁴⁵ R. Yamada,⁴⁵ S. Yang,⁴ T. Yasuda,⁴⁵ Y.A. Yatsunenkov,³¹ W. Ye,⁶⁴ Z. Ye,⁴⁵ H. Yin,⁴⁵ K. Yip,⁶⁵ S.W. Youn,⁴⁵ J.M. Yu,⁵⁶

J. Zennaro,⁶² T.G. Zhao,⁴¹ B. Zhou,⁵⁶ J. Zhu,⁵⁶ M. Zielinski,⁶³ D. Zieminska,⁴⁹ and L. Zivkovic^{p14}

(The D0 Collaboration*)

- ¹LAFEX, Centro Brasileiro de Pesquisas Físicas, Rio de Janeiro, RJ 22290, Brazil
²Universidade do Estado do Rio de Janeiro, Rio de Janeiro, RJ 20550, Brazil
³Universidade Federal do ABC, Santo André, SP 09210, Brazil
⁴University of Science and Technology of China, Hefei 230026, People's Republic of China
⁵Universidad de los Andes, Bogotá, 111711, Colombia
⁶Charles University, Faculty of Mathematics and Physics, Center for Particle Physics, 116 36 Prague 1, Czech Republic
⁷Czech Technical University in Prague, 116 36 Prague 6, Czech Republic
⁸Institute of Physics, Academy of Sciences of the Czech Republic, 182 21 Prague, Czech Republic
⁹Universidad San Francisco de Quito, Quito 170157, Ecuador
¹⁰LPC, Université Blaise Pascal, CNRS/IN2P3, Clermont, F-63178 Aubière Cedex, France
¹¹LPSC, Université Joseph Fourier Grenoble 1, CNRS/IN2P3, Institut National Polytechnique de Grenoble, F-38026 Grenoble Cedex, France
¹²CPPM, Aix-Marseille Université, CNRS/IN2P3, F-13288 Marseille Cedex 09, France
¹³LAL, Univ. Paris-Sud, CNRS/IN2P3, Université Paris-Saclay, F-91898 Orsay Cedex, France
¹⁴LPNHE, Universités Paris VI and VII, CNRS/IN2P3, F-75005 Paris, France
¹⁵CEA Saclay, Irfu, SPP, F-91191 Gif-Sur-Yvette Cedex, France
¹⁶IPHC, Université de Strasbourg, CNRS/IN2P3, F-67037 Strasbourg, France
¹⁷IPNL, Université Lyon 1, CNRS/IN2P3, F-69622 Villeurbanne Cedex, France and Université de Lyon, F-69361 Lyon CEDEX 07, France
¹⁸III. Physikalisches Institut A, RWTH Aachen University, 52056 Aachen, Germany
¹⁹Physikalisches Institut, Universität Freiburg, 79085 Freiburg, Germany
²⁰II. Physikalisches Institut, Georg-August-Universität Göttingen, 37073 Göttingen, Germany
²¹Institut für Physik, Universität Mainz, 55099 Mainz, Germany
²²Ludwig-Maximilians-Universität München, 80539 München, Germany
²³Panjab University, Chandigarh 160014, India
²⁴Delhi University, Delhi-110 007, India
²⁵Tata Institute of Fundamental Research, Mumbai-400 005, India
²⁶University College Dublin, Dublin 4, Ireland
²⁷Korea Detector Laboratory, Korea University, Seoul, 02841, Korea
²⁸CINVESTAV, Mexico City 07360, Mexico
²⁹Nikhef, Science Park, 1098 XG Amsterdam, the Netherlands
³⁰Radboud University Nijmegen, 6525 AJ Nijmegen, the Netherlands
³¹Joint Institute for Nuclear Research, Dubna 141980, Russia
³²Institute for Theoretical and Experimental Physics, Moscow 117259, Russia
³³Moscow State University, Moscow 119991, Russia
³⁴Institute for High Energy Physics, Protvino, Moscow region 142281, Russia
³⁵Petersburg Nuclear Physics Institute, St. Petersburg 188300, Russia
³⁶Institució Catalana de Recerca i Estudis Avançats (ICREA) and Institut de Física d'Altes Energies (IFAE), 08193 Bellaterra (Barcelona), Spain
³⁷Uppsala University, 751 05 Uppsala, Sweden
³⁸Taras Shevchenko National University of Kyiv, Kiev, 01601, Ukraine
³⁹Lancaster University, Lancaster LA1 4YB, United Kingdom
⁴⁰Imperial College London, London SW7 2AZ, United Kingdom
⁴¹The University of Manchester, Manchester M13 9PL, United Kingdom
⁴²University of Arizona, Tucson, Arizona 85721, USA
⁴³University of California Riverside, Riverside, California 92521, USA
⁴⁴Florida State University, Tallahassee, Florida 32306, USA
⁴⁵Fermi National Accelerator Laboratory, Batavia, Illinois 60510, USA
⁴⁶University of Illinois at Chicago, Chicago, Illinois 60607, USA
⁴⁷Northern Illinois University, DeKalb, Illinois 60115, USA
⁴⁸Northwestern University, Evanston, Illinois 60208, USA
⁴⁹Indiana University, Bloomington, Indiana 47405, USA
⁵⁰Purdue University Calumet, Hammond, Indiana 46323, USA
⁵¹University of Notre Dame, Notre Dame, Indiana 46556, USA
⁵²Iowa State University, Ames, Iowa 50011, USA
⁵³University of Kansas, Lawrence, Kansas 66045, USA
⁵⁴Louisiana Tech University, Ruston, Louisiana 71272, USA
⁵⁵Northeastern University, Boston, Massachusetts 02115, USA
⁵⁶University of Michigan, Ann Arbor, Michigan 48109, USA
⁵⁷Michigan State University, East Lansing, Michigan 48824, USA

- ⁵⁸University of Mississippi, University, Mississippi 38677, USA
⁵⁹University of Nebraska, Lincoln, Nebraska 68588, USA
⁶⁰Rutgers University, Piscataway, New Jersey 08855, USA
⁶¹Princeton University, Princeton, New Jersey 08544, USA
⁶²State University of New York, Buffalo, New York 14260, USA
⁶³University of Rochester, Rochester, New York 14627, USA
⁶⁴State University of New York, Stony Brook, New York 11794, USA
⁶⁵Brookhaven National Laboratory, Upton, New York 11973, USA
⁶⁶Langston University, Langston, Oklahoma 73050, USA
⁶⁷University of Oklahoma, Norman, Oklahoma 73019, USA
⁶⁸Oklahoma State University, Stillwater, Oklahoma 74078, USA
⁶⁹Oregon State University, Corvallis, Oregon 97331, USA
⁷⁰Brown University, Providence, Rhode Island 02912, USA
⁷¹University of Texas, Arlington, Texas 76019, USA
⁷²Southern Methodist University, Dallas, Texas 75275, USA
⁷³Rice University, Houston, Texas 77005, USA
⁷⁴University of Virginia, Charlottesville, Virginia 22904, USA
⁷⁵University of Washington, Seattle, Washington 98195, USA

(Dated: March 20, 2017)

We present a combination of measurements of the top quark mass by the D0 experiment in the lepton+jets and dilepton channels. We use all the data collected in Run I (1992–1996) at $\sqrt{s} = 1.8$ TeV and Run II (2001–2011) at $\sqrt{s} = 1.96$ TeV of the Tevatron $p\bar{p}$ collider, corresponding to integrated luminosities of 0.1 fb^{-1} and 9.7 fb^{-1} , respectively. The combined result is: $m_t = 174.95 \pm 0.40$ (stat) ± 0.64 (syst) GeV = 174.95 ± 0.75 GeV.

PACS numbers: 14.65.Ha, 13.85.Ni, 13.85.Qk, 12.15.Ff

I. INTRODUCTION

The top quark is the heaviest known elementary particle with a mass approximately twice that of the electroweak vector bosons, and factor of 1.4 larger than that of the more recently discovered Higgs boson [1]. Within the standard model (SM), this large mass arises from a large Yukawa coupling (≈ 0.9) to the Higgs field. Consequently, loops involving the top quark contribute significantly to electroweak quantum corrections, and therefore a precise measurement of the top quark mass, m_t , provides a means to test the consistency of the SM. Furthermore, the precise values of both the mass of the Higgs boson and the Yukawa coupling of the top quark may play a critical role in the history and stability of the universe

(see e.g., Ref. [2]).

The top quark was discovered in 1995 by the CDF and D0 experiments during Run I (1992–1996) of the Fermilab Tevatron $p\bar{p}$ collider at $\sqrt{s} = 1.8$ TeV [3, 4]. Run II (2001–2011) at $\sqrt{s} = 1.96$ TeV followed, providing a factor of ≈ 150 more top-antitop quark pairs than Run I, and far more precise measurements of m_t . Using $t\bar{t}$ events produced in the D0 detector [5–8], we have measured m_t in different decay channels [9–15] using the full integrated luminosity of Run I ($\int \mathcal{L} dt = 0.1 \text{ fb}^{-1}$) and Run II ($\int \mathcal{L} dt = 9.7 \text{ fb}^{-1}$). This article reports the combination of these direct top quark mass measurements.

Direct measurements of the top quark mass have also been performed by the CDF experiment (see e.g. Ref. [16]) at the Tevatron, and by the ATLAS (see e.g. Ref. [17]) and CMS (see e.g. Ref. [18]) experiments at the CERN LHC. In 2012, the Tevatron experiments combined their measurements in Ref. [19] with the result $m_t = 173.18 \pm 0.94$ GeV. In 2014, a preliminary combination of ATLAS, CDF, CMS, and D0 measurements [20] yielded $m_t = 173.34 \pm 0.76$ GeV. Both combinations are by now outdated as they do not include the latest and more precise measurements, in particular, the final D0 Run II measurements discussed in this article.

The top quark mass is a fundamental free parameter of the SM. However, its definition depends on the scheme of theoretical calculations used for the perturbative expansion in quantum chromodynamics (QCD). The inputs to the combination presented in this article are the direct measurements calibrated using Monte Carlo (MC) simulations. Hence, the measured mass corresponds to the MC mass parameter. However, because of the presence

*with visitors from ^aAugustana College, Sioux Falls, SD 57197, USA, ^bThe University of Liverpool, Liverpool L69 3BX, UK, ^cDeutsches Elektronen-Synchrotron (DESY), Notkestrasse 85, Germany, ^dCONACyT, M-03940 Mexico City, Mexico, ^eSLAC, Menlo Park, CA 94025, USA, ^fUniversity College London, London WC1E 6BT, UK, ^gCentro de Investigacion en Computacion - IPN, CP 07738 Mexico City, Mexico, ^hUniversidade Estadual Paulista, São Paulo, SP 01140, Brazil, ⁱKarlsruher Institut für Technologie (KIT) - Steinbuch Centre for Computing (SCC), D-76128 Karlsruhe, Germany, ^jOffice of Science, U.S. Department of Energy, Washington, D.C. 20585, USA, ^kAmerican Association for the Advancement of Science, Washington, D.C. 20005, USA, ^lKiev Institute for Nuclear Research (KINR), Kyiv 03680, Ukraine, ^mUniversity of Maryland, College Park, MD 20742, USA, ⁿEuropean Organization for Nuclear Research (CERN), CH-1211 Geneva, Switzerland, ^oPurdue University, West Lafayette, IN 47907, USA, and ^pInstitute of Physics, Belgrade, Belgrade, Serbia. [‡]Deceased.

of long range effects in QCD, the relationship between the MC mass and other mass definitions, such as the pole mass or the mass in the modified minimal subtraction ($\overline{\text{MS}}$) scheme, is not well established and has been subject to debate for many years (see e.g., Ref. [21] and references therein). A recent work obtains a difference of +0.6 GeV between the MC mass and the pole mass in the context of an $e^+e^- \rightarrow t\bar{t}$ simulation with an uncertainty of 0.3 GeV [22]. Further studies are needed to produce a similar estimate in the context of $p\bar{p} \rightarrow t\bar{t}$ production.

In Ref. [23], we extracted the pole mass of the top quark from the measured $t\bar{t}$ cross section [24]. However, due to the ambiguity between the MC and pole mass, the difficulty of properly assessing correlations between systematic uncertainties, and the large uncertainty of the pole mass measurement, the latter is not part of the combination presented in this article.

This article is structured as follows: we first summarize the input measurements; we subsequently present the combination of Run II dilepton measurements, which provides one of the inputs to the D0 combination; we then discuss the different uncertainty categories and their correlations, and conclude with the final combined result.

II. DECAY CHANNELS AND INPUT MEASUREMENTS

To measure the top quark mass, we use $p\bar{p} \rightarrow t\bar{t}$ events and assume that the top and antitop quark masses are equal [25–28]. Within the SM, the top quark decays into a W boson and a b quark almost 100% of the time. Different channels arise from the possible decays of the pair of W bosons:

- i. The “dilepton” channel ($\ell\ell'$) corresponds to events ($\approx 4.5\%$ of the total) where both W bosons decay into electrons or muons. This channel is quite free from background but has a small yield. The background is mainly due to Z +jets production, but also receives contributions from diboson (WW , WZ , ZZ), W +jets, and multijet production.
- ii. The “lepton+jets” channel ($\ell + \text{jets}$) corresponds to events ($\approx 30\%$ of the total) where one W boson decays into $q\bar{q}'$ and the other into an electron or a muon and a neutrino. This channel has a moderate yield and a background arising from W +jets production, Z +jets production, and multijet processes.
- iii. The “all jets” channel ($\approx 46\%$ of the total) has events in which both W bosons decay to $q\bar{q}'$ that evolve into jets. The yield is high, but the background from multijet production is very large.
- iv. The “tau channel” ($\approx 20\%$ of the total) arises from events in which at least one of the W bosons decays into $\tau\nu_\tau$. As the decays $\tau \rightarrow \text{hadrons} + \nu_\tau$ are

difficult to distinguish from QCD jets, it is not exploited for the top quark mass measurement. However, the $\tau \rightarrow \ell\nu_\ell\nu_\tau$ decays provide contributions to the $\ell\ell'$ and $\ell + \text{jets}$ channels.

The high mass of the top quark means that the decay products tend to have high transverse momenta (p_T) relative to the beam axis and large angular separations. Reconstructing and identifying $t\bar{t}$ events requires reconstruction and identification of high p_T electrons, muons, and jets, and the measurement of the imbalance in transverse momentum in each event (\cancel{p}_T) due to escaping neutrinos. In addition, identifying b jets is an effective way of improving the purity of the selections. Good momentum resolution is required for all these objects, and the jet energy scale (JES) has to be known with high precision. In the Run II $\ell + \text{jets}$ measurements, the uncertainty in the JES is reduced by performing an in situ calibration, which exploits the $W \rightarrow qq'$ decay by requiring the mass of the corresponding dijet system to be consistent with the mass of the W boson (80.4 GeV). This calibration, determined using light-quark jets (including charm jets), is applied to jets of all flavors associated with $t\bar{t}$ decay. It is then propagated to the Run II $\ell\ell'$ measurements.

The input measurements of m_t for the presented combination are shown in Table I, and consist of measurements performed during Run I and Run II in the $\ell\ell'$ and $\ell + \text{jets}$ channels using the full data sets. D0 also measured the top quark mass using the “all jets” channel in Run I [29]; however, this measurement is not considered in the combination because its uncertainty is large and some subcomponents of the systematic uncertainty are not available. Just as in Run I, two $\ell\ell'$ mass measurements were performed in Run II using a neutrino weighting [12] technique (NW) and a matrix element method (ME) [13]. We discuss their combination in the following section.

To combine the m_t measurements, we use the Best Linear Unbiased Estimate (BLUE) [30], assuming Gaussian uncertainties, both for the $\ell\ell'$ Run II and the final D0 combinations.

III. COMBINATION OF RUN II DILEPTON MEASUREMENTS

In the $\ell\ell'$ channel, the presence of two undetected neutrinos with high p_T makes it impossible to fully reconstruct the kinematics of the final state. To overcome this problem, we use two methods in Run II. The NW measurement [12] is based on a weight function for each event which is computed by comparing the x - and y -components of the observed \cancel{p}_T and the hypothesized p_T components of the neutrinos, integrating over the neutrino pseudorapidities [31]. The maximum weight value indicates the most likely value of m_t in that event. The first and second moments of this function are retained as the event-by-event variables sensitive to m_t . Their distributions in MC events are used to form two-dimensional tem-

TABLE I: Summary of the input measurements to the combination. We indicate the method used to extract the mass of the top quark from the data (see the corresponding references for further details).

Period	Channel	$\int \mathcal{L} dt$ (fb $^{-1}$)	Method	m_t (GeV)	Reference
Run I	$\ell\ell'$	0.1	Combination of matrix weighting and neutrino weighting	168.4 ± 12.3 (stat) ± 3.6 (syst)	[9, 10]
Run I	$\ell + \text{jets}$	0.1	Matrix element	180.1 ± 3.6 (stat) ± 3.9 (syst)	[11]
Run II	$\ell\ell'$	9.7	Neutrino weighting	173.32 ± 1.36 (stat) ± 0.85 (syst)	[12]
Run II	$\ell\ell'$	9.7	Matrix element	173.93 ± 1.61 (stat) ± 0.88 (syst)	[13]
Run II	$\ell + \text{jets}$	9.7	Matrix element	174.98 ± 0.41 (stat) ± 0.63 (syst)	[14, 15]

plates that depend upon the value of m_t . The templates are compared to the data to extract m_t . The ME [13] measurement uses per-event probability densities, based on the reconstructed kinematic information, obtained by integrating over the differential cross sections for the processes contributing to the observed events, using leading order matrix elements for the $t\bar{t}$ production process and accounting for detector resolution. The unmeasured neutrino momentum components are integrated out in this computation. The probability densities from all data events are combined to form a likelihood as a function of m_t , which is then maximized to determine m_t .

A. Statistical uncertainties and correlation

The statistical uncertainties of the individual NW and ME measurements are given in Table II. Both measurements are carried out using the same full D0 Run II data set, and similar selection criteria. Approximately 90% of the selected events are common to both analyses, and the measurements are therefore statistically correlated. We use an ensemble testing method to estimate these correlations. In the first step, we generate 1000 ensembles of simulated background and signal events with mass $m_t = 172.5$ GeV that pass the criteria of either the NW or the ME selection (see Refs. [12] and [13] for the detailed descriptions of the selections). Each ensemble is generated with the same number of events as observed in data, using the expected signal and background fractions, separately for the ee , $\mu\mu$, and $e\mu$ channels. The ME and NW ensembles are then obtained using the individual and slightly more restrictive selection criteria from each analysis, and m_t is extracted following each of the analysis methods. From the two-dimensional distribution of the measured masses shown in Fig 1, we obtain a statistical correlation of $\rho = 0.64 \pm 0.02$ between the two sets of measurements.

B. Systematic uncertainties in $\ell\ell'$ channel

The different contributions to the systematic uncertainty considered in the NW and ME measurements are reported in Table II. The sources of uncertainty are listed in the following and briefly described when the naming is not self-explanatory. More detailed descriptions are

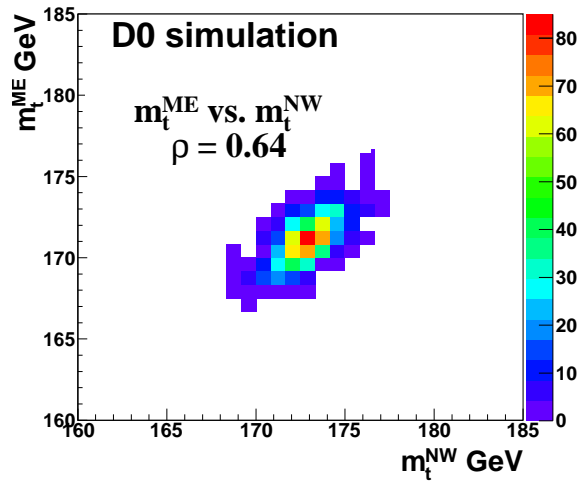


FIG. 1: Two-dimensional distribution in the top quark masses extracted from the MC event ensembles in the ME and NW analyses. The statistical correlation ρ is obtained from this distribution.

given in Refs. [12] and [13], and in Sec. IV for the signal modeling uncertainties.

In situ light-jet calibration: The statistical uncertainty of the JES calibration, determined in the $\ell + \text{jets}$ measurement using light-quark jets, and propagated to the $\ell\ell'$ measurements.

Response to b , q , and g jets: The part of the JES uncertainty that originates from differences in detector response among b , light-quark, and gluon jets.

Model for b jets: The part of the JES uncertainty that originates from uncertainties specific to the modeling of b jets. This includes the dependence on semileptonic branching fractions and modeling of b quark fragmentation.

Light-jet response: The part of the JES uncertainty that affects all jets and includes the dependence of the calibration upon jet energy and pseudorapidity, and the effect of the out-of-cone calorimeter showering correction.

Jet energy resolution

Jet identification efficiency

Multiple interaction model: The systematic uncertainty that arises from modeling the distribution of the number of interactions per Tevatron bunch crossing.

b tag modeling: The uncertainty related to the modeling of the b tagging efficiency for b , c , and light-flavor jets in MC simulation relative to data.

Electron energy resolution

Muon momentum resolution

Lepton momentum scale: The uncertainty arising from the calibration of electron energy and muon momentum scales.

Trigger efficiency: The uncertainties in the estimation of lepton-based trigger efficiencies.

Higher-order corrections: The modeling of higher-order corrections in the simulation of $t\bar{t}$ samples, obtained from the difference between the next-to-leading-order MC@NLO [32] and the leading-order ALPGEN [33] event generators.

Initial and final state radiation: The uncertainty due to the modeling of initial and final state gluon radiation.

Hadronization and underlying events: The uncertainty associated with the modeling of hadronization and the underlying event, estimated from the difference between different hadronization models.

Color reconnection: The uncertainty due to the model of color reconnection.

PDF: The uncertainty from the choice of parton density functions.

Transverse momentum of $t\bar{t}$ system: The uncertainty in the modeling of the distribution of the p_T of the $t\bar{t}$ system.

Yield of vector boson + heavy flavor: The uncertainty associated with the production cross section for $Z+b\bar{b}$ and $Z+c\bar{c}$ relative to Z +jets events.

Background from simulation: The systematic uncertainty on the MC background, which includes the uncertainty from detector effects and the theoretical cross section. It does not include the uncertainties on the ratios of $Z+b\bar{b}$ and $Z+c\bar{c}$ to Z +jets cross sections, which belong to the previous category.

Background based on data: The uncertainties from the modeling of the multijet and W +jets backgrounds estimated using data.

Template statistics: In the NW measurement, this uncertainty arises from the statistical fluctuations of individual bins in signal and background templates. In the ME measurement, there is no such uncertainty as there is no template used to fit the data.

Calibration method: The calibration for both ME and NW measurements is determined using an ensemble testing method. We generate pseudo-experiments with the same number of events as observed in data, using MC events for signal and both MC and data-based samples for backgrounds. Ensembles at different top quark mass hypotheses are generated to determine a linear relation between the uncorrected measurement and the actual MC mass, i.e., to determine slope and offset parameters. The uncertainty in the calibration method arises from the uncertainty in the slope and offset parameters due to the limited size of the MC and data-based samples.

All systematic uncertainties are considered as fully correlated between ME and NW except for the calibration method uncertainty, as the calibrations were performed using almost independent event samples.

The differences between the ME and NW uncertainties reported in Table II are consistent with the expected statistical fluctuations in the various estimates. The fluctuations are ≈ 0.05 – 0.10 GeV, depending on the source, and their overall contributions are well below the total uncertainties. They therefore have a negligible impact on the overall uncertainties in the individual measurements and their combination.

C. $\ell\ell'$ combination

To obtain the ME and NW combination through the BLUE method we use the correlations and uncertainties discussed in Sec. III A and Sec. III B.

The result of the BLUE combination is $m_t = 173.50 \pm 1.31$ (stat) ± 0.84 (syst) GeV. The breakdown of uncertainties is given in Table II. The weights for the NW and ME measurements are 71% and 29%, respectively. The NW and ME measurements agree with a χ^2 of 0.2 for one degree of freedom, corresponding to a probability of 65%. As a test of stability, we change the statistical correlation between the two methods from 0.50 to 0.70 to conservatively cover the range of systematic and statistical uncertainty in its determination. The resulting m_t changes by less than 0.04 GeV.

This combination of the Run II $\ell\ell'$ measurements is used as an input to the overall combination discussed in the next sections.

TABLE II: Measurements in the $\ell\ell'$ channel with contributions to the uncertainties, and their combination. The total systematic uncertainty and the total uncertainty are obtained by adding the relevant contributions in quadrature. All values are given in GeV. The symbol “n/a” stands for “not applicable”.

	Run II	Run II	Run II
	ME	NW	$\ell\ell'$ combination
top quark mass	173.93	173.32	173.50
In situ light-jet calibration	0.46	0.47	0.47
Response to b , q , and g jets	0.30	0.27	0.28
Model for b jets	0.21	0.10	0.13
Light-jet response	0.20	0.36	0.31
Jet energy resolution	0.15	0.12	0.13
Jet identification efficiency	0.08	0.03	0.04
Multiple interaction model	0.10	0.06	0.07
b tag modeling	0.28	0.19	0.22
Electron energy resolution	0.16	0.01	0.05
Muon momentum resolution	0.10	0.03	0.05
Lepton momentum scale	0.10	0.01	0.04
Trigger efficiency	0.06	0.06	0.06
Higher-order corrections	0.16	0.33	0.28
Initial and final state radiation	0.16	0.15	0.15
Hadronization and underlying event	0.31	0.11	0.17
Color reconnection	0.15	0.22	0.20
PDF	0.20	0.08	0.11
Transverse momentum of $t\bar{t}$ system	0.03	0.07	0.06
Yield of vector boson + heavy flavor	0.06	0.04	0.05
Background from simulation	0.06	0.01	0.02
Background based on data	0.07	0.00	0.02
Template statistics	n/a	0.18	0.13
Calibration method	0.03	0.07	0.05
Systematic uncertainty	0.88	0.85	0.84
Statistical uncertainty	1.61	1.36	1.31
Total uncertainty	1.84	1.61	1.56

IV. UNCERTAINTY CATEGORIES IN THE OVERALL COMBINATION

For the overall combination, the systematic uncertainties are grouped into sources of same or similar origin to form uncertainty categories. We employ categories similar to those used in the Tevatron top quark mass combination [19] and use the same naming scheme.

In situ light-jet calibration: The part of the JES uncertainty that originates from the in situ calibration procedure using light-quark jets. This uncertainty has a statistical origin. For the Run II $\ell\ell'$ measurement, the uncertainty from transferring the $\ell + \text{jets}$ calibration to the dilepton event topology is included in the light-jet response category described below.

Response to b , q , and g jets: As described in Sec. III B.

Model for b jets: As described in Sec. III B.

Light-jet response: The part of the JES uncertainty that includes calibrations of the absolute energy-dependent response and the relative η -dependent response, and, for Run II, the out-of-cone calorimeter showering correction. This uncertainty applies to jets of any flavor.

Out-of-cone correction: The part of the JES uncertainty that originates from modeling of uncertainties associated with light-quark fragmentation and out-of-cone calorimeter showering corrections in Run I measurements. For Run II measurements, it is included in the light-jet response category.

Offset: This includes the uncertainty arising from uranium noise in the D0 calorimeter and from the corrections to the JES due to multiple interactions. While such uncertainties were sizable in Run I, the shorter integration time in the calorimeter electronics and the in situ JES calibration make them negligible in Run II.

Jet modeling: The systematic uncertainties arising from uncertainties in jet resolution and identification.

Multiple interactions model: As described in Sec. III B.

b tag modeling: As described in Sec. III B.

Lepton modeling: The uncertainties in the modeling of the scale and resolution of lepton p_T , which were taken to be negligible in Run I.

Signal modeling: The systematic uncertainties arising from $t\bar{t}$ event modeling, which are correlated across all measurements. This includes the sources described below. In Run I, the breakdown into the first four items could not be performed, because the MC generators used at that time did not have the same flexibility as the more modern generators. Instead, the overall signal modeling uncertainty was estimated by changing the main parameters of a MC generator or comparing results from two different generators.

- i. The uncertainty associated with the modeling of initial and final state radiation, obtained by changing the renormalization scale in the scale-setting procedure relative to its default, as suggested in Ref. [34]. Studies of $Z \rightarrow \ell\ell$ data indicate that a range of variation between factors of $\frac{1}{2}$ and 2 of this scale covers the mis-modeling [15].
- ii. The uncertainty from higher-order corrections evaluated from a comparison of $t\bar{t}$ samples generated using MC@NLO [32] and ALPGEN [33], both interfaced to HERWIG [35, 36] for the simulation of parton showers and hadronization.

- iii. The systematic uncertainty arising from a change in the phenomenological description of color reconnection (CR) among final state partons [37]. It is obtained from the difference between event samples generated using PYTHIA [38] with the Perugia 2011 tune and using PYTHIA with the Perugia 2011NOCR tune [39].
- iv. The systematic uncertainty associated with the choice for modeling parton-shower, hadronization, and underlying event. It includes the changes observed when substituting PYTHIA for HERWIG [35, 36] when modeling $t\bar{t}$ signal.
- v. The uncertainty associated with the choice of PDF used to generate the $t\bar{t}$ MC events. It is estimated in Run II by changing the 20 eigenvalues of the CTEQ6.1M PDF [40] within their uncertainties. In Run I, it was obtained by comparing CTEQ3M [41] with MRSA [42] for $\ell\ell'$, and CTEQ4M [43] with CTEQ5L [44] for $\ell + \text{jets}$ events.

Background from theory: This systematic uncertainty on background originating from theory takes into account the uncertainty in modeling the background sources. It is correlated among all measurements in the same channel, and includes uncertainties on background composition, normalization, and distributions.

Background based on data: This includes uncertainties associated with the modeling of multijet background in the $\ell + \text{jets}$ channel, and multijet and $W + \text{jets}$ backgrounds in the $\ell\ell'$ channel, which are estimated using data. This also includes the effects of trigger uncertainties determined from the data.

Calibration method: The uncertainty arising from any source specific to a particular fitting method, includes effects such as the finite number of MC events available to calibrate each method.

Table III summarizes the input measurements and their corresponding statistical and systematic uncertainties.

V. CORRELATIONS

The following correlations are used to combine the measurements:

- i. The uncertainties listed as ‘statistical uncertainty’, ‘calibration method’, and ‘background based on data’ are taken to be uncorrelated among the measurements.
- ii. The uncertainties in the ‘in situ light-jet calibration’ category are taken to be correlated among

the Run II measurements since the $\ell\ell'$ measurement uses the JES calibration determined in the $\ell + \text{jets}$ channel.

- iii. The uncertainties in ‘response to b , q , and g jets’, ‘jet modeling’, ‘ b tag modeling’, ‘multiple interaction model’, and ‘lepton modeling’ are taken to be 100% correlated among Run II measurements.
- iv. The uncertainties in ‘out-of-cone correction’ and ‘offset’ categories are taken to be 100% correlated among Run I measurements.
- v. The uncertainties in ‘model for b jets’ and ‘signal modeling’ categories are taken to be 100% correlated among all measurements.
- vi. The uncertainties in ‘light-jet response’ are taken to be 100% correlated among the Run I and the Run II measurements, but uncorrelated between Run I and Run II.
- vii. The uncertainties in ‘background from theory’ are taken to be 100% correlated among all measurements in the same channel.

A summary of the correlations among the different systematic categories is shown in Table IV. Using the inputs from Table III and the correlations specified in Table IV, we obtain an overall matrix of correlation coefficients in Table V.

VI. RESULTS

We combine the D0 input measurements of Table III using the BLUE method. The BLUE combination has a χ^2 of 2.5 for 3 degrees of freedom, corresponding to a probability of 47%. The pulls and weights for each of the inputs obtained from the BLUE method are listed in Table VI. Here, the pull associated to each input value m_i with uncertainty σ_i is calculated as $\frac{(m_i - m_t)}{\sqrt{\sigma_i^2 - \sigma_{m_t}^2}}$, where $\sigma_{m_t}^2$ is the uncertainty in the combination, and indicates the degree of agreement of the input with the combined value. The weight w_i given to the input measurement m_i is $w_i = \sum_{j=1}^4 (\text{Cov}^{-1})_{ij} / N$, where Cov is the covariance matrix of the input measurements, and N is a normalization term ensuring $\sum_{i=1}^4 w_i = 1$. The covariance matrix expressed in terms of the correlation coefficients between the measurements c_{ij} (with the convention $c_{ii} = 0$) is: $\text{Cov}_{ij} = \sigma_i \sigma_j (\delta_{ij} + c_{ij})$, where δ_{ij} is the Kronecker δ . At first order in the correlation coefficients, its inverse is given by $(\text{Cov}^{-1})_{ij} = \frac{1}{\sigma_i \sigma_j} (\delta_{ij} - c_{ij})$, so that the weight w_i can be written as $w_i = \frac{1}{\sigma_i^2} (1 - \sum_{j \neq i} \frac{\sigma_i}{\sigma_j} c_{ij}) / N'$, N' being a normalization term. This expression shows that the weight for the Run I $\ell\ell'$ measurement is negative mainly because the correlation with the Run II $\ell + \text{jets}$ measurement (0.07) is larger than the ratio of their uncertainties (0.76/12.7).

TABLE III: Summary of measurements used to determine the D0 average m_t . Integrated luminosity ($\int \mathcal{L} dt$) has units of fb^{-1} , and all other values are in GeV. The uncertainty categories and their correlations are described in Sec. IV. The total systematic uncertainty and the total uncertainty are obtained by adding the relevant contributions in quadrature. The symbol “n/a” stands for “not applicable”, and the symbol “n/e” for “not evaluated” (but expected to be negligible).

	D0 Run I		D0 Run II	
	$\ell + \text{jets}$	$\ell\ell'$	$\ell + \text{jets}$	$\ell\ell'$
$\int \mathcal{L} dt$	0.1	0.1	9.7	9.7
top quark mass	180.10	168.40	174.98	173.50
In situ light-jet calibration	n/a	n/a	0.41	0.47
Response to b , q , and g jets	n/e	n/e	0.16	0.28
Model for b jets	0.71	0.71	0.09	0.13
Light-jet response	2.53	1.12	0.21	0.31
Out-of-cone correction	2.00	2.00	n/a	n/a
Offset	1.30	1.30	n/a	n/a
Jet modeling	n/e	n/e	0.07	0.14
Multiple interaction model	n/e	n/e	0.06	0.07
b tag modeling	n/e	n/e	0.10	0.22
Lepton modeling	n/e	n/e	0.01	0.08
Signal modeling	1.10	1.80	0.35	0.43
Background from theory	1.00	1.10	0.06	0.05
Background based on data	n/e	n/e	0.09	0.06
Calibration method	0.58	1.14	0.07	0.14
Systematic uncertainty	3.89	3.63	0.63	0.84
Statistical uncertainty	3.60	12.30	0.41	1.31
Total uncertainty	5.30	12.83	0.76	1.56

TABLE IV: Summary of correlations among sources of uncertainty. The symbols \times or \otimes within any category indicate the uncertainties that are 100% correlated. The uncertainties marked as \times are uncorrelated with those marked as \otimes . The symbol 0 indicates absence of correlations. The symbol “n/a” stands for “not applicable”.

	D0 Run I		D0 Run II	
	$\ell + \text{jets}$	$\ell\ell'$	$\ell + \text{jets}$	$\ell\ell'$
In situ light-jet calibration	n/a	n/a	\times	\times
response to b , q , and g jets	n/a	n/a	\times	\times
Model for b jets	\times	\times	\times	\times
Light-jet response	\otimes	\otimes	\times	\times
Out-of-cone correction	\times	\times	n/a	n/a
Offset	\times	\times	n/a	n/a
Jet modeling	n/a	n/a	\times	\times
Multiple interactions model	n/a	n/a	\times	\times
b tag modeling	n/a	n/a	\times	\times
Lepton modeling	n/a	n/a	\times	\times
Signal modeling	\times	\times	\times	\times
Background from theory	\times	\otimes	\times	\otimes
Background based on data	n/a	n/a	0	0
Calibration method	0	0	0	0
Statistical	0	0	0	0

The resulting combined value for the top quark mass is

$$m_t = 174.95 \pm 0.40 (\text{stat}) \pm 0.64 (\text{syst}) \text{ GeV}.$$

Adding the statistical and systematic uncertainties in quadrature yields a total uncertainty of 0.75 GeV, corre-

TABLE V: The matrix of correlation coefficients used to determine the D0 average top quark mass.

	Run I,	Run I,	Run II,	Run II,
	$\ell + \text{jets}$	$\ell\ell'$	$\ell + \text{jets}$	$\ell\ell'$
Run I, $\ell + \text{jets}$	1.00			
Run I, $\ell\ell'$	0.16	1.00		
Run II, $\ell + \text{jets}$	0.13	0.07	1.00	
Run II, $\ell\ell'$	0.07	0.05	0.43	1.00

TABLE VI: The pull and weight for each input channel when using the BLUE method to determine the average top quark mass.

	D0 Run I		D0 Run II	
	$\ell + \text{jets}$	$\ell\ell'$	$\ell + \text{jets}$	$\ell\ell'$
Pull	0.98	-0.51	0.63	-1.06
Weight	0.002	-0.003	0.964	0.035

sponding to a relative precision of 0.43% on the top quark mass. The breakdown of the uncertainties is shown in Table VII. The dominant sources of uncertainty are the statistical uncertainty, the JES calibration, which has statistical origin, and the modeling of the signal. The total statistical and systematic uncertainties are reduced relative to the published D0 and CDF combination [19] due primarily to the latest and most accurate D0 $\ell + \text{jets}$ analysis [14, 15]. As a test of stability, we vary the correlation of the dominant source of uncertainties, ‘signal modeling’, from 100% to 0%, first between Run I and Run II measurements, and in a second check between all measurements. The combined value of m_t does not change by more than 50 MeV, while the uncertainty changes by no more than 20 MeV. This is due to the fact that the Run II $\ell + \text{jets}$ measurement dominates the combination with a weight of 96%. Thus, the combination is not sensitive to the detailed description of the correlation of systematic uncertainties. Due to a much smaller total uncertainty resulting in the large weight for the $\ell + \text{jets}$ measurement, the improvement in the combined uncertainty relative to the individual $\ell + \text{jets}$ uncertainty is smaller than 10 MeV.

The input measurements and the resulting D0 average mass of the top quark are summarized in Fig. 2, along with the top quark pole mass extracted by D0 from the measurement of the $t\bar{t}$ cross section [23].

VII. SUMMARY

We have presented the combination of the measurements of the top quark mass in all D0 data. Taking into account the statistical and systematic uncertainties and their correlations, we find a combined average of $m_t = 174.95 \pm 0.75 \text{ GeV}$. This measurement with, a relative precision of 0.43%, constitutes the legacy Run I

TABLE VII: Combination of D0 measurements of m_t and contributions to its overall uncertainty. The uncertainty categories are defined in the text. The total systematic uncertainty and the total uncertainty are obtained by adding the relevant contributions in quadrature.

	D0 combined values (GeV)
top quark mass	174.95
In situ light-jet calibration	0.41
Response to b , q , and g jets	0.16
Model for b jets	0.09
Light-jet response	0.21
Out-of-cone correction	< 0.01
Offset	< 0.01
Jet modeling	0.07
Multiple interaction model	0.06
b tag modeling	0.10
Lepton modeling	0.01
Signal modeling	0.35
Background from theory	0.06
Background based on data	0.09
Calibration method	0.07
Systematic uncertainty	0.64
Statistical uncertainty	0.40
Total uncertainty	0.75

and Run II measurement of the top quark mass in the D0 experiment.

VIII. ACKNOWLEDGMENTS

We thank the staffs at Fermilab and collaborating institutions, and acknowledge support from the Depart-

ment of Energy and National Science Foundation (United States of America); Alternative Energies and Atomic Energy Commission and National Center for Scientific Research/National Institute of Nuclear and Particle Physics (France); Ministry of Education and Science of the Russian Federation, National Research Center “Kurchatov Institute” of the Russian Federation, and Russian Foundation for Basic Research (Russia); National Council for the Development of Science and Technology and Carlos Chagas Filho Foundation for the Support of Research in the State of Rio de Janeiro (Brazil); Department of Atomic Energy and Department of Science and Technology (India); Administrative Department of Science, Technology and Innovation (Colombia); National Council of Science and Technology (Mexico); National Research Foundation of Korea (Korea); Foundation for Fundamental Research on Matter (The Netherlands); Science and Technology Facilities Council and The Royal Society (United Kingdom); Ministry of Education, Youth and Sports (Czech Republic); Bundesministerium für Bildung und Forschung (Federal Ministry of Education and Research) and Deutsche Forschungsgemeinschaft (German Research Foundation) (Germany); Science Foundation Ireland (Ireland); Swedish Research Council (Sweden); China Academy of Sciences and National Natural Science Foundation of China (China); and Ministry of Education and Science of Ukraine (Ukraine).

-
- [1] G. Aad *et al.* (ATLAS and CMS Collaborations), Combined Measurement of the Higgs Boson Mass in pp Collisions at $\sqrt{s} = 7$ and 8 TeV with the ATLAS and CMS Experiments, *Phys. Rev. Lett.* **114**, 191803 (2015).
 - [2] G. Degross, S. Di Vita, J. Elias-Miro, J. R. Espinosa, G. F. Giudice, G. Isidori, and A. Strumia, Higgs mass and vacuum stability in the Standard Model at NNLO, *J. High Energy Phys.* **08**, 098 (2012).
 - [3] F. Abe *et al.* (CDF Collaboration), Observation of top quark production in $\bar{p}p$ collisions, *Phys. Rev. Lett.* **74**, 2626 (1995).
 - [4] S. Abachi *et al.* (D0 Collaboration), Observation of the top quark, *Phys. Rev. Lett.* **74**, 2632 (1995).
 - [5] S. Abachi *et al.* (D0 Collaboration), The D0 detector, *Nucl. Instrum. Methods Phys. Res., Sect. A* **338**, 185 (1994).
 - [6] V. M. Abazov *et al.* (D0 Collaboration), The upgraded D0 detector, *Nucl. Instrum. Methods Phys. Res., Sect. A* **565**, 463 (2006).
 - [7] M. Abolins *et al.*, Design and implementation of the new D0 level-1 calorimeter trigger, *Nucl. Instrum. Methods Phys. Res., Sect. A* **584**, 75 (2008).
 - [8] R. Angstadt *et al.* (D0 Collaboration), The layer 0 inner silicon detector of the D0 experiment, *Nucl. Instrum. Methods Phys. Res., Sect. A* **622**, 298 (2010).
 - [9] B. Abbott *et al.* (D0 Collaboration), Measurement of the top quark mass using dilepton events, *Phys. Rev. Lett.* **80**, 2063 (1998).
 - [10] B. Abbott *et al.* (D0 Collaboration), Measurement of the top quark mass in the dilepton channel, *Phys. Rev. D* **60**, 052001 (1999).
 - [11] V. M. Abazov *et al.* (D0 Collaboration), A precision measurement of the mass of the top quark, *Nature* **429**, 638 (2004).
 - [12] V. M. Abazov *et al.* (D0 Collaboration), Precise measurement of the top quark mass in dilepton decays using optimized neutrino weighting, *Phys. Lett. B* **752**, 18 (2016).
 - [13] V. M. Abazov *et al.* (D0 Collaboration), Measurement of the Top Quark Mass Using the Matrix Element Technique in Dilepton Final States, *Phys. Rev. D* **94**, 032004 (2016).
 - [14] V. M. Abazov *et al.* (D0 Collaboration), Precision measurement of the top-quark mass in lepton+jets final

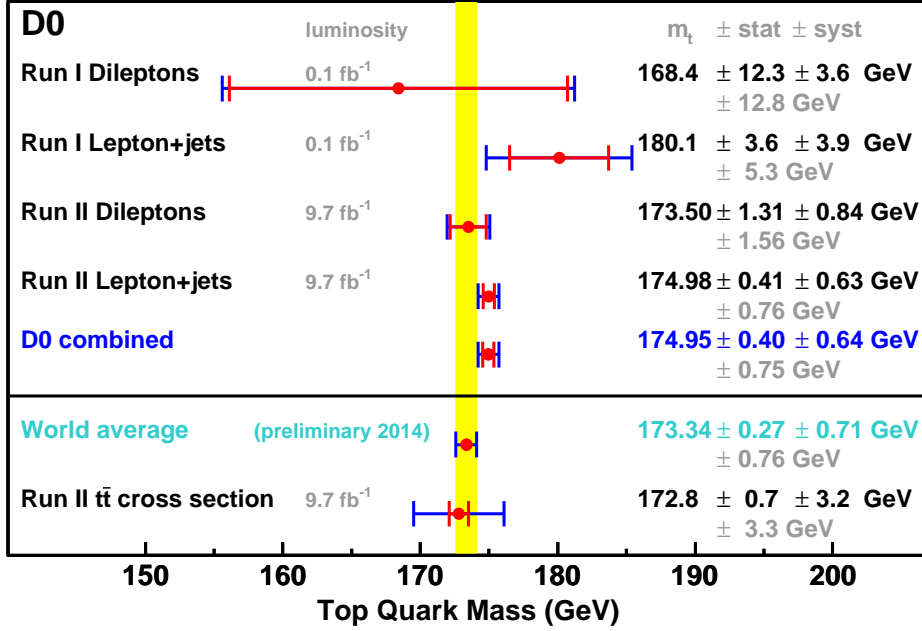


FIG. 2: A summary of the top quark mass measurements used in the D0 combination [9–15], along with the D0 final result, and the top quark pole mass extracted from the D0 cross section measurement [23]. The latter is not used in the combination. The inner red uncertainty bars represent the statistical uncertainties, while the blue bars represent the total uncertainties. For comparison, we also show the preliminary 2014 world average of m_t [20] which includes D0 Run II $\ell\ell'$ and $\ell + \text{jets}$ measurements that are now superseded. For the top quark pole mass extracted from the D0 cross section measurement, a 1.1 GeV theory uncertainty is included in the systematic uncertainty, and the statistical uncertainty is determined such as its relative contribution to the experimental uncertainty is the same as for the cross-section measurement.

- states, Phys. Rev. Lett. **113**, 032002 (2014).
- [15] V. M. Abazov *et al.* (D0 Collaboration), Precision measurement of the top-quark mass in lepton+jets final states, Phys. Rev. D **91**, 112003 (2015).
- [16] T. Aaltonen *et al.* (CDF Collaboration), Precision Top-Quark Mass Measurements at CDF, Phys. Rev. Lett. **109**, 152003 (2012).
- [17] M. Aaboud *et al.* (ATLAS Collaboration), Measurement of the top quark mass in the $t\bar{t} \rightarrow$ dilepton channel from $\sqrt{s} = 8$ TeV ATLAS data, Phys. Lett. B **761**, 350 (2016).
- [18] V. Khachatryan *et al.* (CMS Collaboration), Measurement of the top quark mass using proton-proton data at $\sqrt{s} = 7$ and 8 TeV, Phys. Rev. D **93**, 072004 (2016).
- [19] T. Aaltonen *et al.* (CDF and D0 Collaborations), Combination of the top-quark mass measurements from the Tevatron collider, Phys. Rev. D **86**, 092003 (2012).
- [20] G. Aad *et al.* (ATLAS, CDF, CMS, and D0 Collaborations), First combination of Tevatron and LHC measurements of the top-quark mass (2014), arXiv:1403.4427.
- [21] A. Juste, S. Mantry, A. Mitov, A. Penin, P. Skands, E. Varnes, M. Vos, and S. Wimpenny, Determination of the top quark mass circa 2013: methods, subtleties, perspectives, Eur. Phys. J. C **74**, 3119 (2014).
- [22] M. Butenschoen, B. Dehnadi, A. H. Hoang, V. Mateu, M. Preisser, and I. W. Stewart, Top Quark Mass Calibration for Monte Carlo Event Generators, Phys. Rev. Lett. **117**, 232001 (2016).
- [23] V. M. Abazov *et al.* (D0 Collaboration), Measurement of the inclusive $t\bar{t}$ production cross section in $p\bar{p}$ collisions at $\sqrt{s} = 1.96$ TeV and determination of the top quark pole mass, Phys. Rev. D **94**, 092004 (2016).
- [24] U. Langenfeld, S. Moch, and P. Uwer, Measuring the running top-quark mass, Phys. Rev. D **80**, 054009 (2009).
- [25] V. M. Abazov *et al.* (D0 Collaboration), Direct measurement of the mass difference between top and antitop quarks, Phys. Rev. D **84**, 052005 (2011).
- [26] T. Aaltonen *et al.* (CDF Collaboration), Measurement of the mass difference between top and antitop quarks, Phys. Rev. D **87**, 052013 (2013).
- [27] G. Aad *et al.* (ATLAS Collaboration), Measurement of the mass difference between top and anti-top quarks in pp collisions at $\sqrt{s} = 7$ TeV using the ATLAS detector, Phys. Lett. B **728**, 363 (2014).
- [28] S. Chatrchyan *et al.* (CMS Collaboration), Measurement of the mass difference between top quark and antiquark in pp collisions at $\sqrt{s} = 8$ TeV, Phys. Lett. B **770**, 50 (2017).
- [29] V. M. Abazov *et al.* (D0 Collaboration), Measurement of the top quark mass in all-jet events, Phys. Lett. B **606**, 25 (2005).
- [30] A. Valassi, Combining correlated measurements of several different physical quantities, Nucl. Instrum. Methods Phys. Res., Sect. A **500**, 391 (2003).
- [31] The D0 coordinate system is right-handed, with the z -axis pointing in the direction of the Tevatron proton beam and the y -axis pointing upwards. The pseudorapidity is defined as $\eta = -\ln(\tan\theta/2)$, where θ is the polar angle relative to z -axis.
- [32] S. Frixione and B. R. Webber, Matching NLO QCD computations and parton shower simulations, J. High Energy Phys. **06**, 029 (2002).
- [33] M. L. Mangano, F. Piccinini, A. D. Polosa, M. Moretti, and R. Pittau, ALPGEN, a generator for hard multiparton processes in hadronic collisions, J. High Energy Phys. **07**, 001 (2003).
- [34] B. Cooper, J. Katzy, M. L. Mangano, A. Messina, L. Mijovic, and P. Skands, Importance of a consistent choice of $\alpha(s)$ in the matching of AlpGen and Pythia, Eur. Phys. J. C **72**, 2078 (2012).
- [35] G. Marchesini, B. R. Webber, G. Abbiendi, I. G. Knowles, M. H. Seymour, and L. Stanco, HERWIG: A Monte Carlo event generator for simulating hadron emission reactions with interfering gluons. Version 5.1 - April 1991, Comput. Phys. Commun. **67**, 465 (1992).
- [36] G. Corcella, I. G. Knowles, G. Marchesini, S. Moretti, K. Odagiri, P. Richardson, M. H. Seymour, and B. R. Webber, HERWIG 6: an event generator for hadron emission reactions with interfering gluons (including supersymmetric processes), J. High Energy Phys. **01**, 010 (2001).
- [37] P. Z. Skands and D. Wicke, Non-perturbative QCD effects and the top mass at the Tevatron, Eur. Phys. J. C **52**, 133 (2007).
- [38] T. Sjostrand, S. Mrenna, and P. Z. Skands, PYTHIA 6.4 physics and manual, J. High Energy Phys. **05**, 026 (2006).
- [39] P. Z. Skands, Tuning Monte Carlo Generators: The Perugia Tunes, Phys. Rev. D **82**, 074018 (2010).
- [40] P. M. Nadolsky, H.-L. Lai, Q.-H. Cao, J. Huston, J. Pumplin, D. Stump, W.-K. Tung, and C. P. Yuan, Implications of CTEQ global analysis for collider observables, Phys. Rev. D **78**, 013004 (2008).
- [41] H. L. Lai, J. Botts, J. Huston, J. G. Morfin, J. F. Owens, J.-W. Qiu, W. K. Tung, and H. Weerts, Global QCD analysis and the CTEQ parton distributions, Phys. Rev. D **51**, 4763 (1995).
- [42] A. D. Martin, W. J. Stirling, and R. G. Roberts, Parton distributions of the proton, Phys. Rev. D **50**, 6734 (1994).
- [43] H. L. Lai, J. Huston, S. Kuhlmann, F. I. Olness, J. F. Owens, D. E. Soper, W. K. Tung, and H. Weerts, Improved parton distributions from global analysis of recent deep inelastic scattering and inclusive jet data, Phys. Rev. D **55**, 1280 (1997).
- [44] H. L. Lai, J. Huston, S. Kuhlmann, J. Morfin, F. I. Olness, J. F. Owens, J. Pumplin, and W. K. Tung (CTEQ), Global QCD analysis of parton structure of the nucleon: CTEQ5 parton distributions, Eur. Phys. J. C **12**, 375 (2000).